

**Estimation of the Intensities of Historical Seismic Events
in Moderately Seismic Regions, Based on the Damage
Analysis of Hungarian Historical Buildings**

Thesis Brochure

Eduardo José de Azevedo Charters Fuentes Morais

Supervisors:

Dr. László Gergely Vigh

Associate Professor

Dr. János Krähling

University Professor



Budapest University of Technology and Economics

Faculty of Civil Engineering

Department of Structural Engineering

2018



Index

1. Introduction	2
1.1. Problem Statement.....	2
1.2. Motivation and Background	3
1.3. Solution Strategy and Interdisciplinary Approach.....	3
2. Magnitude Estimation - Scientific and Theoretical Background	4
3. Historical Research, Descriptions and Architecture.....	5
4. Archetypes Generation.....	8
5. Numerical Model Development and Analysis	10
6. Damage Assessment and Statistics	13
7. Development of the Stochastic Models.....	15
8. Magnitude Estimates for the 1763 Komárom Earthquake	17
9. New Scientific Results	21
9.1. Thesis I	21
9.2. Thesis II	21
9.3. Thesis III.....	21
9.4. Thesis IV	22
9.5. Thesis V.....	22
9.6. Thesis VI	23
Contributions of the Author	24
References	25

1. Introduction

1.1. Problem Statement

In regions of low-to-moderate seismicity, as Hungary, the amount of seismic records for seismic hazard analysis and the list of earthquake is relatively small. Nonetheless, many significant destructive seismic events have occurred before instrumental seismology, as the 1763 earthquake in Komárom [1-3]. The impact of the intensities and magnitude of these historical events, on the hazard models is significant [4, 5] (Fig. 1). For this reason, seismologists and historians have cooperated for historical earthquake research enhancing the lists and magnitude estimates for historical seismic events [6, 7]. The 1763 Komárom earthquake was one of the most destructive seismic events in Hungarian history, and although its damage on buildings is reported in historical sources [9, 10], both its magnitude and epicenter have been disputed in literature, in between 5.7 and 6.5 [1-3].

Although, traditional approaches in seismology evaluate the seismic damage in the light of intensity scales, such as the *Medvedev-Sponheuer-Karnik Scale* (MSK-64) [8], using empirical relationships relating those intensities to the magnitude in order to achieve the final estimates [4]. As a result, the structural behaviour of the buildings affected by the earthquake is left out of deeper considerations.

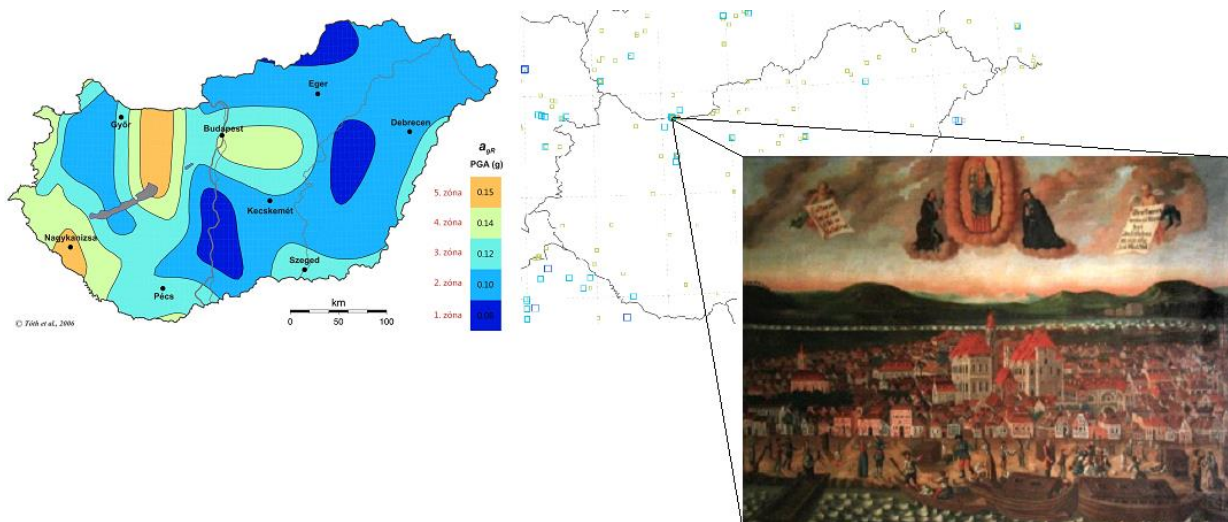


Fig. 1 – Hazard map for Hungary [5] (left), Historical Earthquakes in Hungary [3] (center), and depiction of the damage in the city of Komárom, by an anonymous painter (right).

Another method uses knowledge of the behaviour of structures to determine the magnitude of the seismic events based on structural fragility functions [11]. The method uses structural fragility functions, describing the probability of damage measure (DM) observations given an intensity measure (IM), magnitude (M) and distance (R), and combines it with the seismic events' structural damage records, in order to describe a probability of the damage event E given IM , M and R . Afterwards, it uses an attenuation model $f_{M/M,R}$ and a prior distribution of distance f_R , together with the total probability theorem to describe the probability of occurrence of the damage event E given M . Finally, it employs the Bayes' theorem together with a prior distribution of magnitude f_M to attain the posterior distribution of M given E , as well as the expected value of magnitude and respective standard deviation. A flowchart of the method is presented in Fig. 2. The present dissertation focusses on the method in [11] to estimate the magnitude of the 1763 Komárom earthquake.

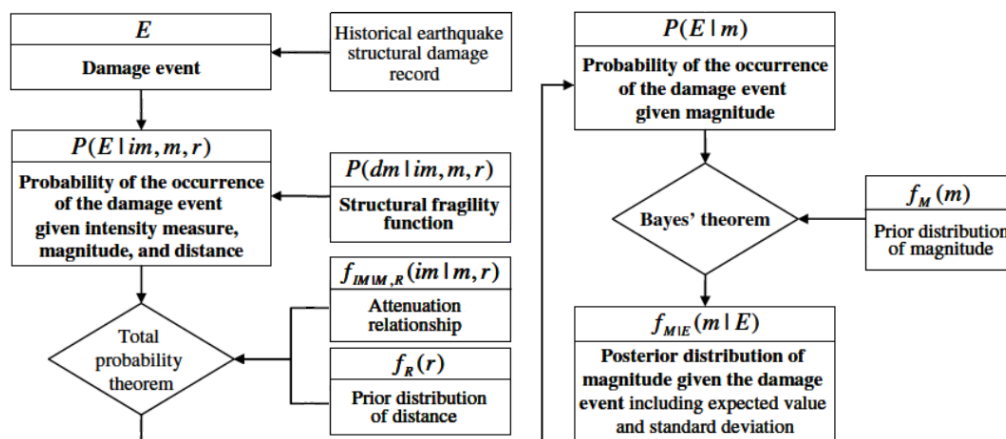


Fig. 2 – Flowchart of the probability for the magnitude estimation [11].

1.2. Motivation and Background

The great advantage this method [11] is that the knowledge of the regional seismicity may be improved since the knowledge of the structural behaviour is added to earlier estimates, possibly enhancing the hazard models and maps. It is also relevant to define the type of the future buildings and seismic safety design/retrofit that will be employed, or how urban arrangement is defined, and both this issues have a profound impact in the economy. The areas of Komárom and Mór are defined by zone 5 in the Hungarian hazard map (Fig. 1). The 1763 earthquake was one of the decisive arguments for stopping the construction of a water powerplant at Nagymaros, on the Danube River, in 1989 [7].

Additionally, the interdisciplinary nature of the research touches interesting topics:

- *Historical research*: research of sources, palaeography and historical demography.
- *History of Architecture*: theory and history of construction systems and protection of monuments.
- *Seismology*: Historical earthquake research techniques and SHA.
- *Mathematics*: parametric problems and uncertainty, probability theory, Bayesian epistemology.
- *Structural and Earthquake Engineering*: historical construction materials, numerical methods for structures, and seismic design and modelling.

Most of them are trends in the long run as the application of probability theory to structural engineering and seismic analysis, but also topics as the protection and monitoring of the cultural heritage. The use of historical research and data to improve the knowledge of modern systems is also a subject of research in applied sciences. The development of structural fragility functions for structures and components under extreme actions has been a field of research at the Structural Engineering Department in BME [EC3].

1.3. Solution Strategy and Interdisciplinary Approach

The application of the method [11] requires an interdisciplinary approach. In order to establish the proposed solution in firm grounds the research finds on empirical data and knowledge of both the historical and modern data on the structural damage and the knowledge of the buildings structures affected by the 1763 earthquake. These two must be interrelated and accounted for in the structural modelling, both in quality and quantity. Therefore, besides investigating the structural damage historical sources, sources of historical buildings research are also explored, with focus on the use of historical buildings surveys (HBS) in the region of Komárom [12, 13]. Afterwards, a database is created from the HBS targeting the 18th c. buildings with the help of literature from the field of History of Architecture [14-16], and their geometrical quantitative data is computed. The geometrical data is synthesized using the inplane



vulnerability indices for historical masonry buildings [17, 18], together with feasible material and load parameters, both as a preliminary indicator of the seismic performance of the historical buildings, and a quantitative framework for the development of historical building archetypes (HBAs). The development of HBAs is carried out with additional interpretation of both the survey and literature of historical buildings research.

In Fig. 3 we provide an overview of the impact the historical earthquake research on vulnerability/risk analysis [19]. The key points can be identified also in Fig. 2, although the magnitude estimation method in [11] inverts this scheme, utilizing the seismic vulnerability described by the fragility curves and combines them with the historical damage records. Just afterwards the source zone and the attenuation models are utilized to model both the ground motion (GM) intensities and magnitude.

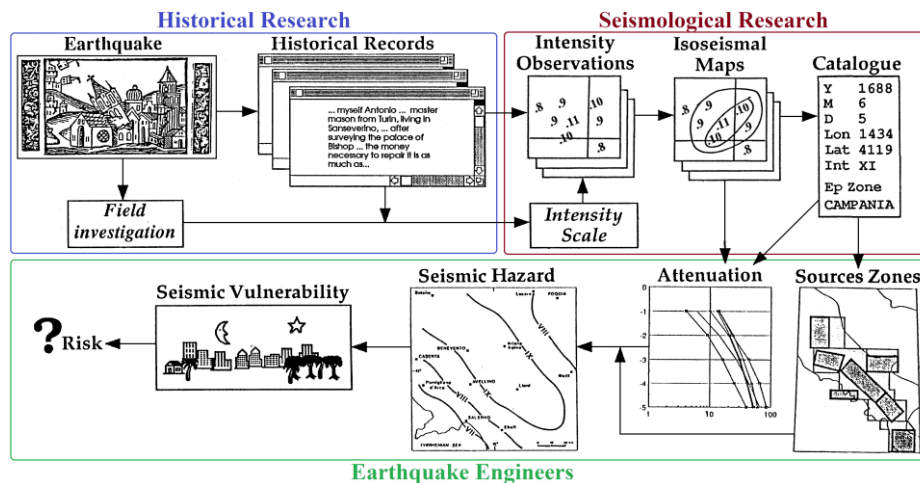


Fig. 3 – General scheme of processing and using macroseismic data for the assessment of seismic hazard and risk [19].

Once the HBAs are created, they are modelled and analysed using both simplified and sophisticated structural [earthquake] engineering *Nonlinear Static* and *Dynamic Structural Analysis* (NSA and DSA, respectively) techniques and softwares [20-29]. The models should not only provide efficient nonlinear simulation but also incorporate the uncertainty in both seismic hazard, load [30-32] and strength parameters [33-36]. This is mostly because historical unreinforced masonry (URM) buildings present modelling difficulties, not only due to the variety of failure modes, possible equilibrium configurations of the assemblies and sensitivity to seismic actions [17], but also due to the lack of evidence and studies on the material strength, despite [35, 37]. Monte-Carlo simulation is an alternative to generate sub-structures with different sets of parameters for analysis [38]. Logical trees are also employed in order to incorporate epistemic uncertainties. Finally, the magnitudes are estimated by the application of [11], and by confronting different sets of assumptions, also to understand the layout of the city of Komárom and of the county.

2. Magnitude Estimation - Scientific and Theoretical Background

The method [11] opens the field of historical earthquake research to the contribution of architecture historians and structural/earthquake engineers with knowledge on the modelling of historical buildings. While the approaches hold fundamental differences, they also have common grounds. The *European Macroseismic Scale EMS-98* [39] uses the idea of seismic vulnerability associated to building classes for damage interpretation, providing a common interface for both seismologists and engineers, relating intensity grades/values and damages in buildings.



Structural fragility functions in Eq (1), typically assumed to be lognormally distributed, describe the conditional probability of observing a certain damage measure DM , with instances dm_k , (with $k=\{0,1,2,\dots,n\}$), given a set of parameters θ , and may well represent the seismic vulnerability.

$$P(DM \geq dm_k | \theta) = \Phi \left(\frac{\ln(X_\theta / \mu_\theta)}{\beta_\theta} \right) \quad (1)$$

where X_θ is the θ parameters' range, μ_θ the median β_θ the standard deviation. The set of parameters θ_i is here composed by a ground motion intensity im .

Hence, the probability of a certain damage measure $P(DM=dm_k|\theta)$ are defined piecewise by Eq. (2).

$$P(DM = dm_k | im) = \begin{cases} 1 - P(DM \geq dm_1 | im) & k = 0 \\ P(DM \geq dm_k | im) - P(DM \geq dm_{k+1} | im) & 1 \leq k \leq n_d - 1 \\ P(DM \geq dm_{n_d} | im) & k = n_d \end{cases} \quad (2)$$

The probability of E given im , m and r , may be described, in this work, Eq. (3), by the occurrence of n damages dm_l in a total of n_t structures:

$$P(E | im, m, r) = \frac{n_t!}{n!(n_t - n)!} \times P(DM = dm_1 | im, m, r)^n \times P(DM = dm_0 | im, m, r)^{n_t - n} \quad (3)$$

or by Eq. (4), describing the probability of occurring n_k damages with in different measures dm_k :

$$P(E | im, m, r) = P \left(\bigcap_{k=0}^{n_d} \binom{j N_k = j n_k}{im, m, r} \right) = \frac{n_t!}{\prod_{k=0}^{n_d} n_k!} \times \prod_{k=0}^{n_d} P(DM=dm_k | im, m, r)^{n_k} \quad (4)$$

The operation of combining the probability of observing damage with the actual historical damage caused by the damage event E , determines the likelihood of the damage event. Afterwards, the total probability theorem, Eq. (5), integrates this probability with an attenuation relationship $f_{IM|M,R}$ and a prior distribution of distance f_R to calculate the probability of the event E given a m , $P(E|m)$:

$$P(E|m) = \iint P(E | im, m, r) \times f_{IM|M,R}(im|m, r) \times f_R(r) \dim dr \quad (5)$$

Finally, the Bayes' theorem, in Eq. (6) computes the likelihood of the damage event E given magnitude m and a prior magnitude distribution f_M , to calculate the posterior/updated distribution of magnitude $f_{M|E}$. The marginal probability of the event E would be $P(E)=\int P(E|m) \cdot f_M dm$:

$$f_{M|E} = \frac{P(E|m) \cdot f_M}{P(E)} \quad (6)$$

The expected value of maganitude and respective standard deviation can be calculated by assuming an unknown distribution, using the total representation theorem:

$$\mu_{M|E} = E \left[\mu_{M|E,M,R} \right] \quad \& \quad \sigma_{M|E} = \sqrt{E \left[\sigma_{M|E,M,R}^2 \right] + \sigma^2 \left[\mu_{M|E,M,R} \right]} \quad (7)$$

where the expected value may be calculated as $E[X|\theta]=\int X \cdot f_{X|\theta} dm$.

3. Historical Research, Descriptions and Architecture

The research of Réthly Antal [40] is seminal, inspiring later works [1, 2, 4, 5, 6]. These works have a curious antecedent in [10], as the author was also an eyewitness of the 1763 earthquake. They also identified early sources on the 1763 earthquake. Contemporary and later sources consist of documents, newspaper articles and manuscripts that constitute as sources of the 1763 event and may be consulted in the National Archives (OL) and National Library (NK):

- *A Komáromi foldrengetes 1763*, article by Gregorics Gábor (NK, 1892), *Komáromi Lapok*;



- *Adatok a komáromi földrengések idejéből*, article by Molnár E. (NK, 1899), in *Komáromi Hirlap*;
- *Szigeti György tudósítása az 1763-dik évi komáromi földrengésről*, article by Szigeti György (NK, 1872) in *Magyar Protestans Figyelo*;
- *Adatok az 1763-iki nagy földrengéshez*, by Rovács Albin (NK, 1902) in *Komáromi Lapok*;
- *A komáromi nagy földindulás 1763 evben*, by Székely Pál (1878) in *Komárom*;
- *Comentatio de tristissimo L. R. Civitatis Comaromiensis terrae motu 1763*, manuscript by Kastenholz Honorius Vilmos (NK, 1763);
- *A Komáromi föld-indulásról* (NK, 1789);
- *Comaromiensis Civitatis terrae motu devastatae brevis historia*, manuscript (NK, 1763).

The report of the Royal Council [9], Grossinger's book [10] and the visual sources (Fig. 4), present the most complete and suggestive sources:

- *Acta terrae motus anni 1763*, report and letters from the *Royal Council* [9];
- *Dissertatio de terrae motus regni Hungarica*, book by Grossinger [10];
- *Damages of Győr*, depicted by Mainzell (1763) [4].

Votiv painting by unknown artist (1766) [4]



Engraving in copper, by János Fülöp (1766)



Earthquake in Komárom in the year 1763, by Friedl (1720,1763) [4]



Damages of Komárom, by József Kastner (1763) [6]



Fig. 4 – Depictions and engravings representing the damage in the city of Komárom.

Karl Friedl's depiction (Fig. 4, up right) was originally painted in 1720 and overpainted after the 1763 earthquake [8], and despite criticism, the damage representations are arguably consistent between depictions. At first glance all four depictions represent the damage in the Jesuit's church and college, mainly in the towers, a similar damage to that represented for Győr. The gables, evident in both Kastner's drawing and the votiv painting [7], and both the votiv and Friedl's paintings represent in detail different instances of collapsed gables, sliding shear, diagonal and rocking cracks (Fig. 5 & Fig. 6).



Fig. 5 – The house with displaced roof [8] (left) and overturned gables (right).

One difficulty in straightforward interpretation of the sources is the high complexity and interaction of failure modes that may arise in masonry assemblies during the earthquake.

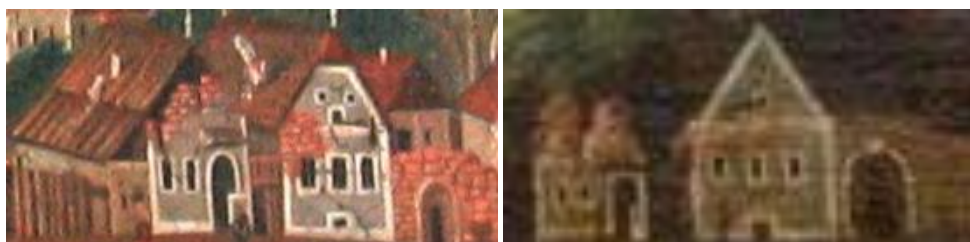


Fig. 6 – House group with evidences of collapsed gable and possibly shear and/or rocking on the walls.

Komárom was extensively damaged – out of 1169 houses in total, 279 ended completely destroyed, 353 partially collapsed, 213 needed expensive repair and 219 cheap repair – in 91% of the houses [4]. Due reserves to the historical expression “collapse”, that may not represent our current, or EMS-98, conception [6]. The damage reports [9] provide relevant macroseismic data for sitematization [2]. This includes the Komárom county, mentioning repair costs and damage numbers, and beyond, with qualitative but useful damage descriptions. The common houses showed more seismic resistance than the stiffer, heavier and probably taller brick public, ecclesiastical and city houses of the town possibly with multiple stories, more embellishment and perhaps vaulted constructions [10].

Despite early efforts to investigate monumental buildings as sources for the magnitude estimates [EC1, EC9], such buildings are underrepresented in the damage sets in comparison to common dwellings. The research turned to historical building surveys (HBS) that are representative of the region and period of the earthquake. The HBS of the city of Tata [12] covers a considerable part of the 18th c. Tata and Tóvaros. After the analysis of the plans and literature, a final list of 34 buildings is shown in Fig. 7:

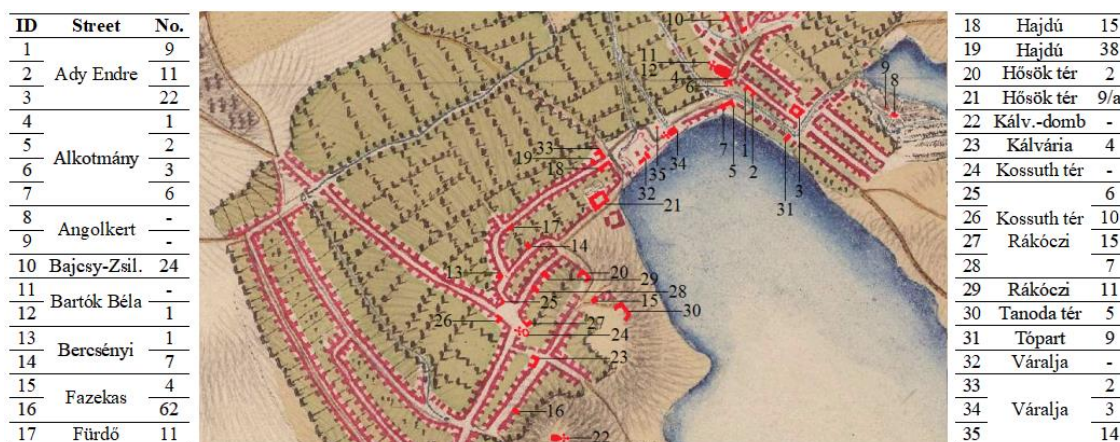


Fig. 7 – Location of the surveyed buildings in the First Military Map (1763-1787) [41, EC10].



The representativeness is bounded to the damage sources and their respective categories but also to architecture, materials and techniques that influenced the original state of the buildings. The building categories were harmonized between sources [9, 12] (Fig. 8, left). It is still a question if the quantities can be extrapolated, yet they seem to be related to the evidenced construction features and techniques. The typologies from building stock of the city of Tata are generally characterized by baroque URM buildings. The main structural elements are masonry walls, with or without openings, vaulted or not, and with wooden roofing systems. The great majority of the surveyed buildings (91.2%) is low-rise – one or two storeys high – with or without basement. From the total number of buildings 11.8% possess a basement. From the total number of taxpayer houses 33% are one-storey and the remaining, 66% two-storey.

The majority of the houses of the town belonged to local peasants and were built of adobe, possibly with flexible willow-twigs; their constructions may also be of mud walls. The foundation structure on which the walls were built was just the well-rammed earth [EC2]. This data is in conformity with the map presented in that singles adobe, and rammed-earth or mud in $\pm 90\%$ of the buildings in the region [35].

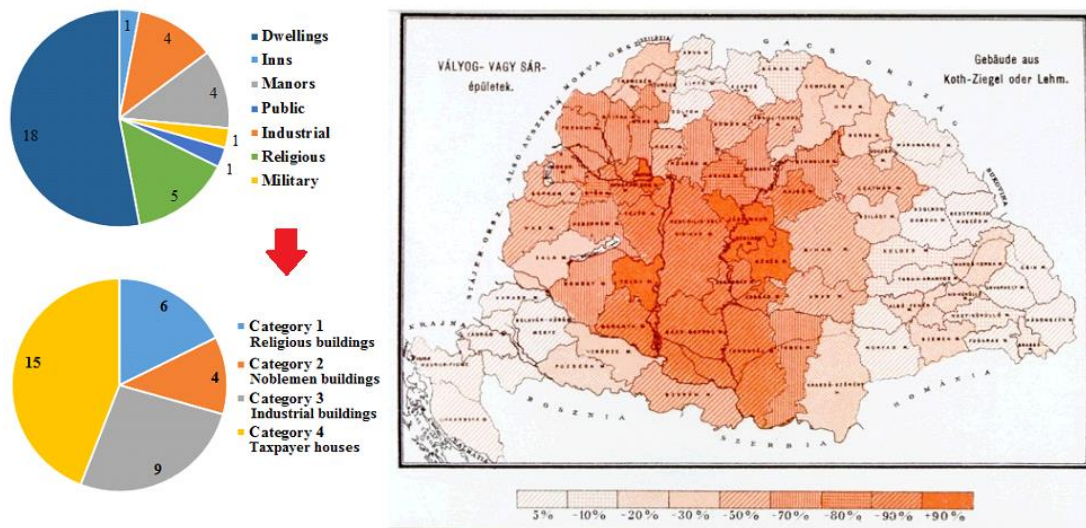


Fig. 8 – Category harmonization (left) and adobe and mud houses in Hungarian Kingdom, from [35].

4. Archetypes Generation

The methodology aims for a comprehensive and flexible qualitative and quantitative approach, based on [17, 18], for the generation of HBAs for seismic analysis [EC6, EC10] using HBS [12] (Fig. 9).

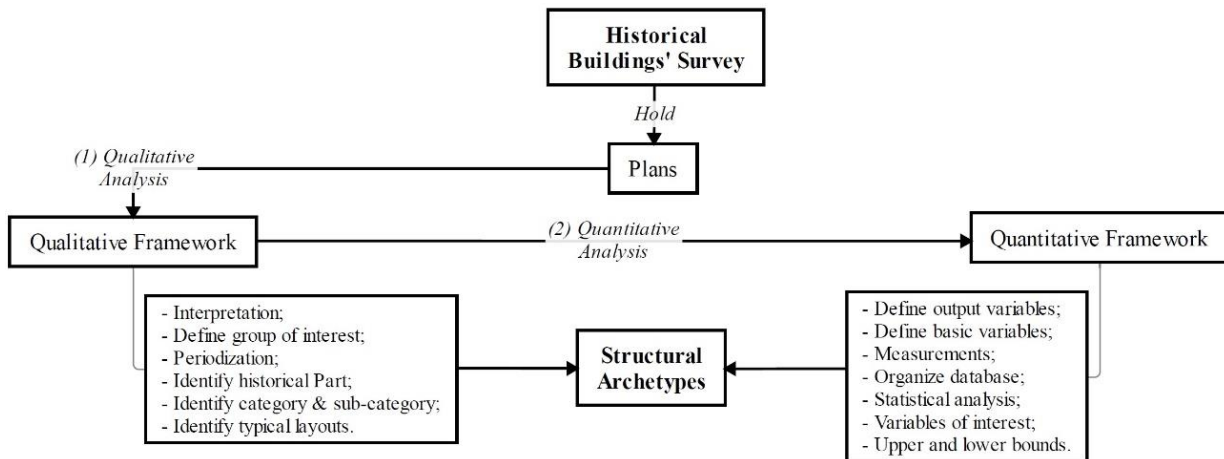


Fig. 9 – Description of the methodology for archetype generation, based on [EC6].



The qualitative analysis is necessarily bounded by the detail/type of survey: (1) true-to-form approach [13], (2) general approach [EC6, EC10], (3) expert opinion [11, EC2], (4) historical plans, or by general literature review. Additionally, it states the guiding principles for building selection and identification the features of interest, as walls (w/, wo/ openings), arches, vaults, although the walls are the main earthquake resisting system, matching both the depictions and descriptions mentioned. The quantitative analysis utilizes the measurements statistics and the in-plane indices [17, 18] to produce HBA befitting seismic analysis. The in-plane area ratio $\gamma_{1,i}$, the area to weight-ratio $\gamma_{2,i}$ and the base shear ratio $\gamma_{3,i}$, Eq. (8):

$$\gamma_{1,i} = \frac{A_{w,i}}{S} = k_1 \times \frac{A_{w,i}}{A_{w,tot}} \geq 1.0 \quad \gamma_{2,i} = \frac{A_{w,i}}{G} = k_2 \times \frac{A_{w,i}}{A_{w,tot}} \geq 1.2 \quad \gamma_{3,i} = \frac{F_{Rm,i}}{F_{Em}} = k_3 \times \frac{A_{w,i}}{A_{w,tot}} \geq 1.0 \quad (8)$$

with $A_{w,tot}=A_{w,x}+A_{w,y}$, $k_1=A_{w,tot}/S$, $k_2=A_{w,tot}/G$ and $k_3=[\tan\phi+f_{vk0}/(\gamma\times G)]/\beta$.

Where the index $\gamma_{1,dir}$ is related to the base shear strength and it is the quotient between the in-plane area of the resistant walls ($A_{w,i}$) and the total in-plane area (S). As to $\gamma_{2,dir}$, it is given by the horizontal cross-section per unit of weight and it is the quotient between the in-plane area of the resistant walls ($A_{w,i}$) and the quasi-permanent vertical action (G). The index $\gamma_{3,dir}$ provides the safety value with respect to shear and it is the quotient between the seismic action ($F_E=\beta\times G$) and the shear strength of the structure ($V_{Rd,base}=F_{Rd}$), being β the equivalent seismic static coefficient.

One paradigmatic example fro the approach is the dwelling house with the ID 2 in Ady Endre Street 11, Tata (Fig. 10, right), using a general approach. This building maintained some of its earlier features, making it possible to identify the baroque walls. From the L-shaped dwelling, three intervention periods may be identified, leading to the conclusion that the probable 18th century wall was preserved in the N-W wing of the building. The existence of a division in the characteristically baroque mansard roof and ellipsoidal windows, in this wing also confirms this hypothesis. Furthermore, the existence of vaulted spaces and a basement suggests that this is probably the oldest part of perhaps a three-cell house, which may be represented by the archetype A0 (Fig. 10, left).

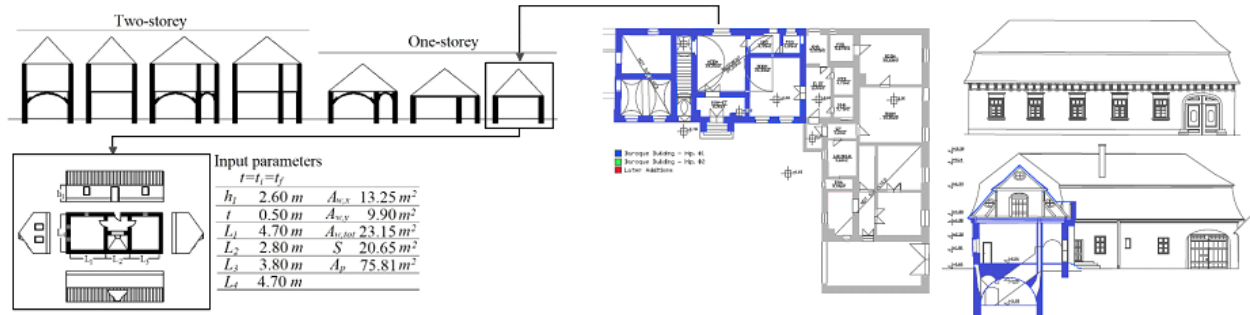


Fig. 10 – Archetype A0, with geometric inputs (left), and dwelling house of Ady Endre Street 11 (right) [12].

Once the earlier building is identified, the measurements of the wall elements and plan areas are processed and the table with the input values for the case study can be presented (Table 1). The selected input variables do not consider only the calculation of the indices, but maximum and minimum thicknesses (t_{min} and t_{max}) and lengths (L_{min} and L_{max}).

Table 1
Input parameters for the in-plan indices calculation for the Ady Endre 11 dwelling.

ID	h	$t=t_i$						$t=t_f$				
		t_{min}	t_{max}	L_{min}	L_{max}	$A_{w,x}$	$A_{w,y}$	$A_{w,tot}$	S	A_p		
2	3.80	0.50	0.57	1.84	4.75	19.84	22.74	42.58	38.00	165.77	90.90	444.23



Additionally, other inputs, material parameters are assumed for comparison. Thus, using the Eq. (8) and the geometrical input parameters in Table 2, the in-plan indices ($\gamma_{i,dir}$) may be calculated, as can be seen in Table 2. As the differences endorse modifications in the height of archetype A0, hence A1.

Table 2
Output parameters and in-plan indices for the Ady Endre 11 dwelling and for the Archetype A0.

ID	Parameters			In-plan area ratio		Area to weight ratio		Base shear ratio	
	k_1	k_2	k_3	$\gamma_{1,x}$	$\gamma_{1,y}$	$\gamma_{2,x}$	$\gamma_{2,y}$	$\gamma_{3,x}$	$\gamma_{3,y}$
2	1.12	14.62	2.51	0.60	0.52	7.81	6.81	1.22	1.07
A0	1.12	21.37	2.19	0.64	0.48	12.23	9.14	2.90	2.17

Additionally, the process described for ID2 was employed with the full HBS statistics for the 4 building categories. The comparison of the results and distinction of the material parameters of adobe (cat. 4) and clay URM, provided the basis for a preliminary vulnerability assessment, with the buildings from categories 1, 2 and 3 relatively lower values for the base shear ratio γ_3 , as well as two-storey buildings of cat. 4, then one-storey cat. 4 buildings. Historical claims seem to agree. One explanation for the resilience may be the low height to weight ratio (due to geometry and specific weight) rather than their strength. Another explanation is higher flexibility of adobe, which can not be judged by this level of analysis.

The full statistics also layed the grounds to generate other archetypes. The new HBA were generated with parametrical adaptation to the indices similarly to A0. These archetypes result from additional interpretation considering both socio-economic and geographical conditions together with the categorization and literature, endorsing the importance of assembling an archetype of a peasant house, which is highly representative of the built environment, of a mill (A6) mainly because of the existence of the lake and canals which source a considerable number of mills. It is also considered a multi-category archetype, which is adaptable to become either a city house (A2), or an inn (A3), or a noblemen house (A4) or a parish house (A5), depending on the adapted parameters (Fig. 11).

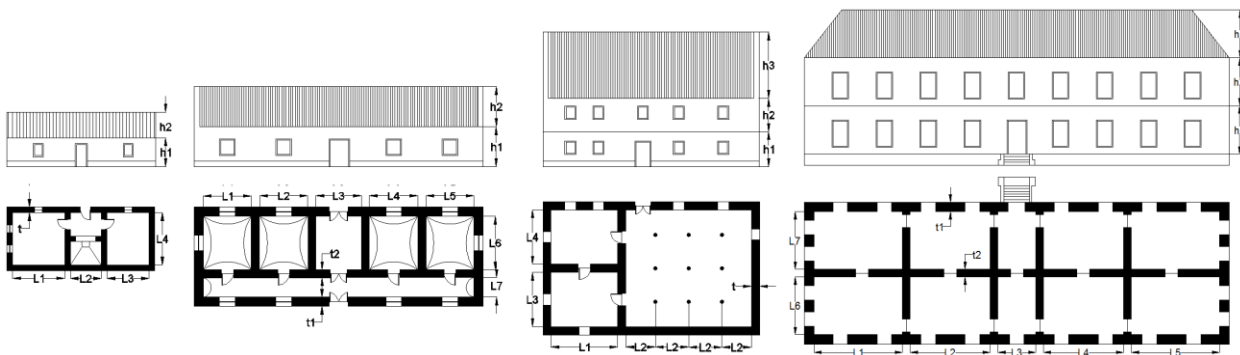


Fig. 11 - Geometries for archetypes of a peasant house (left), multi-category (center left), of a mill (center right) and of a nobleman's house (right).

5. Numerical Model Development and Analysis

The modelling and nonlinear analysis of the structures and damage of the HBAs involved the Geometrical and structural modelling of both planar and spatial models. In a preliminary phase only archetypes A0 and A1 were studied. The unfolding of their walls of the reveals 11 wall panels with different geometrical dimensions, with and without openings (Fig. 12), that may be studied directly as walls (approach 1) or subdivided in macroelements (approach 2).

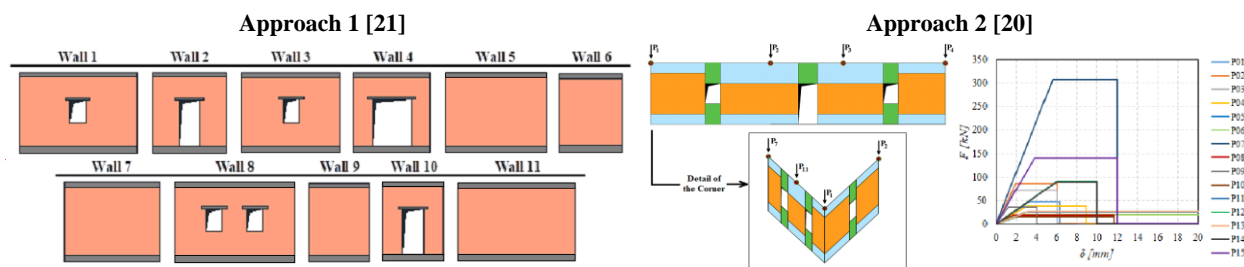


Fig. 12 – Walls of the peasant house archetypes A0/A1 and possible modelling approaches [EC2, EC5].

The geometrical modelling of the Archetypes A0 to A7 was developed in *3Muri* environment, an EFM based code, with post edition of the scripts (Fig. 13).

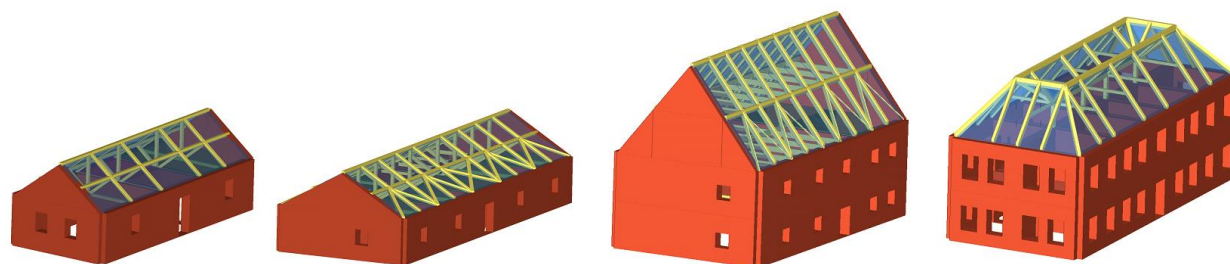


Fig. 13 – Views of the geometric models of the archetypes A0 (similar to A1), A2 (similar to A3, A4 and A5), A6 and A7.

The material modelling is a key issue for achieving a realistic simulation of URM buildings behaviour, therefore different material models were employed for preliminary studies [21, 24, 25]. Nevertheless, *Tremuri* [22] showed an efficient compromise between modelling sophistication and computation speed. It uses the EFM with both shear and rocking models with parameters: specific weight γ , Young modulus E , Poisson ratio ν , compressive strength f_m , shear strength f_v , and different ultimate drift ratios for shear and flexure, $(\delta/h)_v$ and $(\delta/h)_f$, respectively. Although, the material parameter sets for historical masonry varies considerably in literature, even within the same type and technique, being difficult to establish clear bounds and simplified relationships [34, 36, 44, 46]. This data in Hungary is scarce or not adjusted to the time frame [35, 37, 45]. Nevertheless, different feasible ranges of parameters were studied, associated, also, with different building categories and masonry types (inputs in Table 3).

Table 3

Physical and strength parameters for the archetypes A0-to-A7 in four major classes. Units: kN/m³ and MPa

Classes	1		2		3		4		Distribution type
Archetypes	A0, A1 & A2		A3		A4 & A6		A5 & A7		
Parameters	μ_x	σ_x	μ_x	σ_x	μ_x	σ_x	μ_x	σ_x	
γ	16.00	-	17.00	-	17.00	-	18.00	-	-
E	155.00	100.00	200.00	50.00	350.00	100.00	1375.00	500.00	LN
ν	0.20	0.05	0.20	0.05	0.20	0.05	0.20	0.05	N
f_m	1.00	0.75	1.50	0.90	2.35	1.00	4.00	1.50	LN
f_v	0.090	0.015	0.100	0.070	0.500	0.100	0.350	0.100	LN
$G(E,\nu)$	64.58	-	83.33	-	145.83	-	572.91	-	expression
$(\delta/L)_v$	0.53%	0.16%	0.53%	0.16%	0.53%	0.16%	0.53%	0.16%	N
$(\delta/L)_f$	1.07%	0.43%	1.07%	0.43%	1.07%	0.43%	1.07%	0.43%	N

Simplified macro-modelling for dynamic analysis was studied using the ‘Pinching4’ uniaxial and multilinear material model was employed [EC2], in *OpenSees* [23]. Its multilinear backbone allows the simulation of cyclic degradation, here associated to URM behaviour (Fig. 14). Its calibration and validation procedures may employ from sophisticated to simplified analysis methods, so far as they produce backbone diagrams, afterwards the degradation may be adjusted.

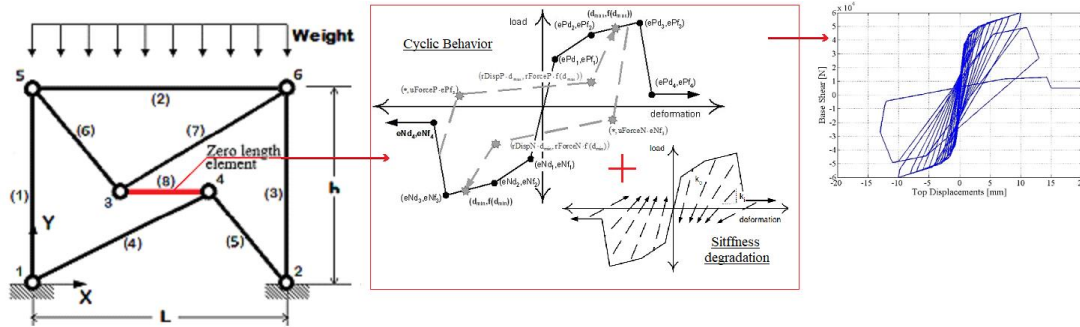


Fig. 14 – *OpenSees* “pinching4” uniaxial material model associated to a planar macromodel [EC2].

The load modelling followed the combination for seismic loading and prescriptions from [42, 43] considering permanent and live loads. A specific attenuation model employed a logic tree to overcome the epistemic uncertainty associated with the use of SHARE [30] (40%) and Paks II [31, EC11] (60%) models. The studied region is characterized by a strike-slip faulting systems and shallow earthquakes occurrence in the top 15 km of the crust, most with Z_{hyp} in between 6 to 9 km [1]. The soil categories B2 (40%), C1 (5%), C2 (45%) and C3 (10%) are plausible, according to [48], with V_{s30} ranging from 200 to 800 m/s, and in harmony with the V_{s30} map for Hungary [47, EC11] (Fig. 15).

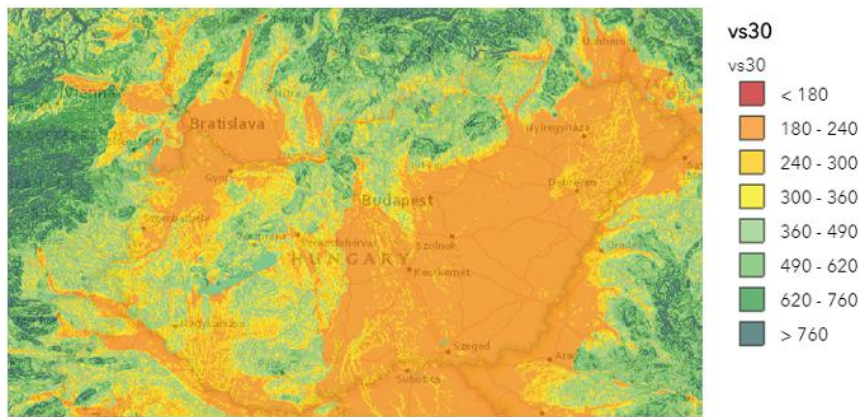


Fig. 15 – V_{s30} map for Hungary [47].

The hazard model was utilized for seismic record selection in the PEER NGA-West2 database [49] was utilized for to select 3 bins of GMRs within the magnitude intervals of interest $5 \leq M_w \leq 6$, $6 \leq M_w \leq 7$ and $7 \leq M_w \leq 8$, with with Joyner-Boore distances $0 \leq R_{JB} \leq 25$ km and strike-slip fault type. The mean spectra and GMRs are displayed in Fig. 16.

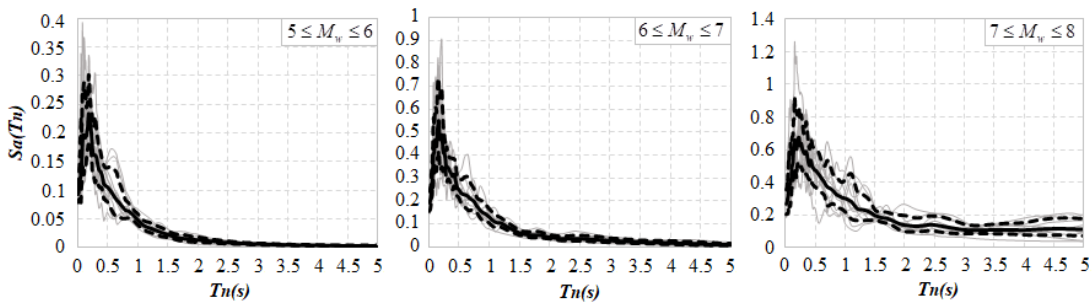


Fig. 16 – Mean Spectra $\mu_{IM} \pm \beta_{IM}$ and selected GMRs.



The spatial models of the HBA, from A0 to A7 were modelled in *Tremuri* [22] and discretized into macroelements: piers, spandrels, and rigid nodes (Fig. 17).

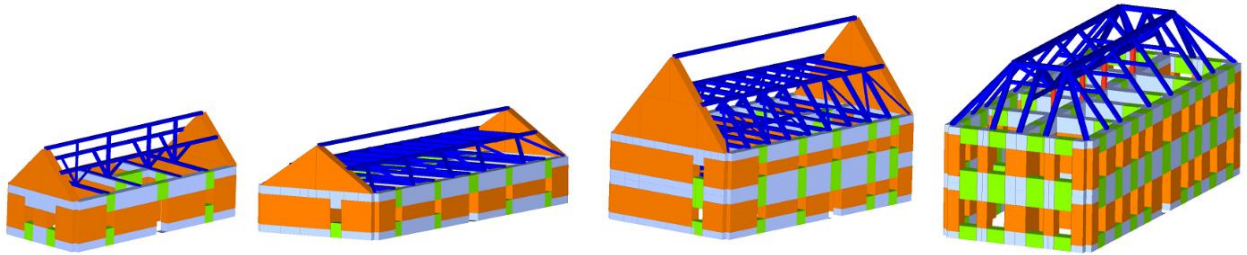


Fig. 17 – Views of the mechanical models of the archetypes A0 (similar to A1), A2 (similar to A3, A4 and A5), A6 and A7.

6. Damage Assessment and Statistics

The simplified and global models of the archetypes were also developed for analysis. The results, namely in force-displacement ($F-\delta$) diagrams, with the objective of describing the damage in buildings represented by the archetypes. The studies of simplified nonlinear analysis involved confronting empirical [21] and semi-empirical models [20] vs FEM modelling [25, EC5]. The study revealed expected discrepancies between walls but the similar range of values for the maximum forces (Fig. 18).

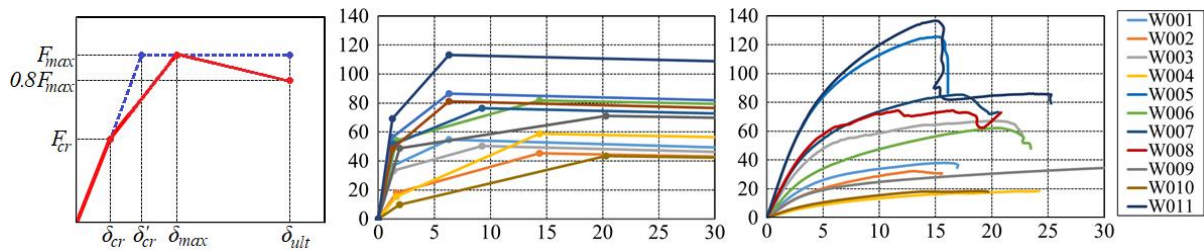


Fig. 18 – Walls’s F- δ backbone: conceptual scheme (left), empirical (centre) & numerical (right) experiment in ATENA [EC5].

The nonlinear static [pushover] analysis (NSA) of the Archetypes was processed in both *3Muri* and *TreMuri Ricerca* [22], resulting in fully developed monotonic curves describing the different damage stages in the two main directions (Fig. 19) using the mean values of the material parameters. The red diagrams draw an equivalent bilinear model of equal collapse energy, with secant stiffness. The damage in the archetypes can be seen using *3Muri* interface also in Fig. 19, where A0 shows the typical predominance of shear mechanisms in the piers, with occasional occurrences of rocking.

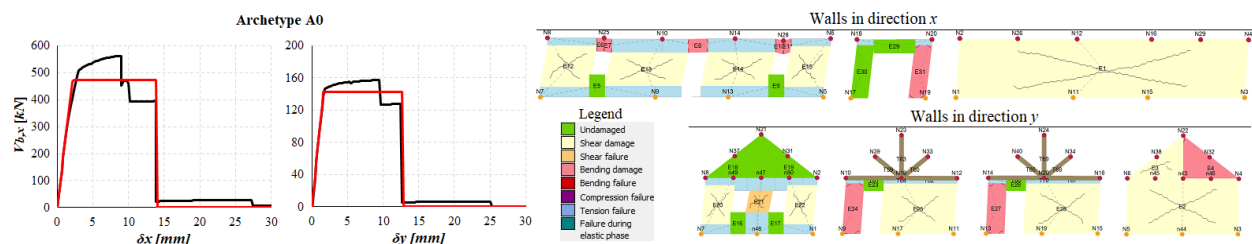


Fig. 19 - Pushover results and damage in archetype A0 (similar to A1).

The backbones of the hysteretic curves were drawn in order to establish the comparison with the corresponding monotonic curves obtained through static pushover analysis. The Model Calibration utilized a genetic algorithm (GA) [50] in order to understand and simulate the cyclic degradation of URM in the hysteretic diagrams with the fittest individuals (Fig. 20, down). Afterwards, the damage statistics were drawn using NSA of the archetypes in order to describe the variability of the material parameters and fol-



lowing the distributions in Table 3, and establish the interpretation and definition of the damage states. The diagrams are displayed in terms of displacements δ , and force-mass ratio V_b/M , where V_b is the base shear force (Fig. 21). The mass for A0 is equal to 112.20 tons.

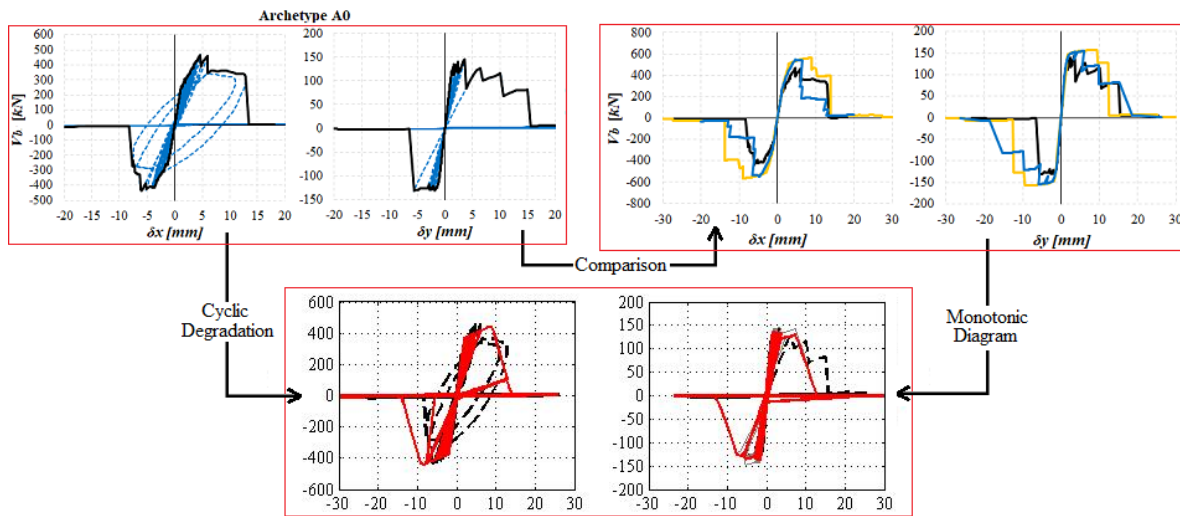


Fig. 20 – The dynamic analysis (up left) comparison with static analysis (up right) and scheme for calibration with GA, for A0.

Damage interpretation, definition and systematization of the damage interpretation can be achieved using the signifiative points. The result is an idealized tetralinear $F-\delta$ diagram that may be used for DSA, and employed by the macromodel presented above in Fig. 14.

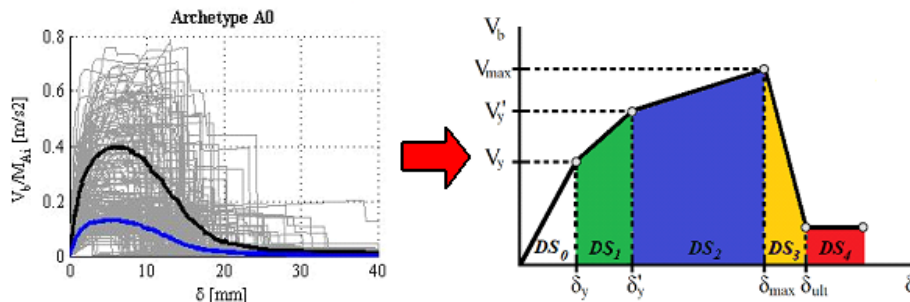
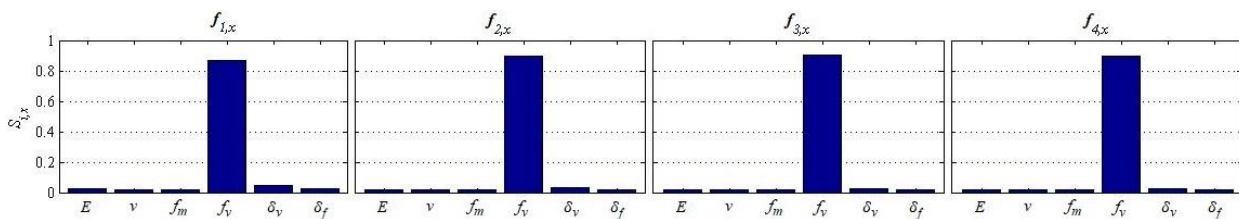


Fig. 21 – Static pushover analysis of the Archetype A0, with respective means for x and y directions (black and blue, respectively, left), and diagram of the damage interpretation scheme (right).

The sensitivity analysis was carried on the idealized backbone curves identifying the significative points of the $F-\delta$ diagrams, in order to evaluate the sensitivity to the random material parameters. The results are paradigmatic in A0 and A7 displayed in Fig. 22. The results show that the shear drift is relevant for the deformability in both A0 and A7, although, for the forces, the shear is relevant only for A0, where for A7 is mostly shared between shear and rocking modes.



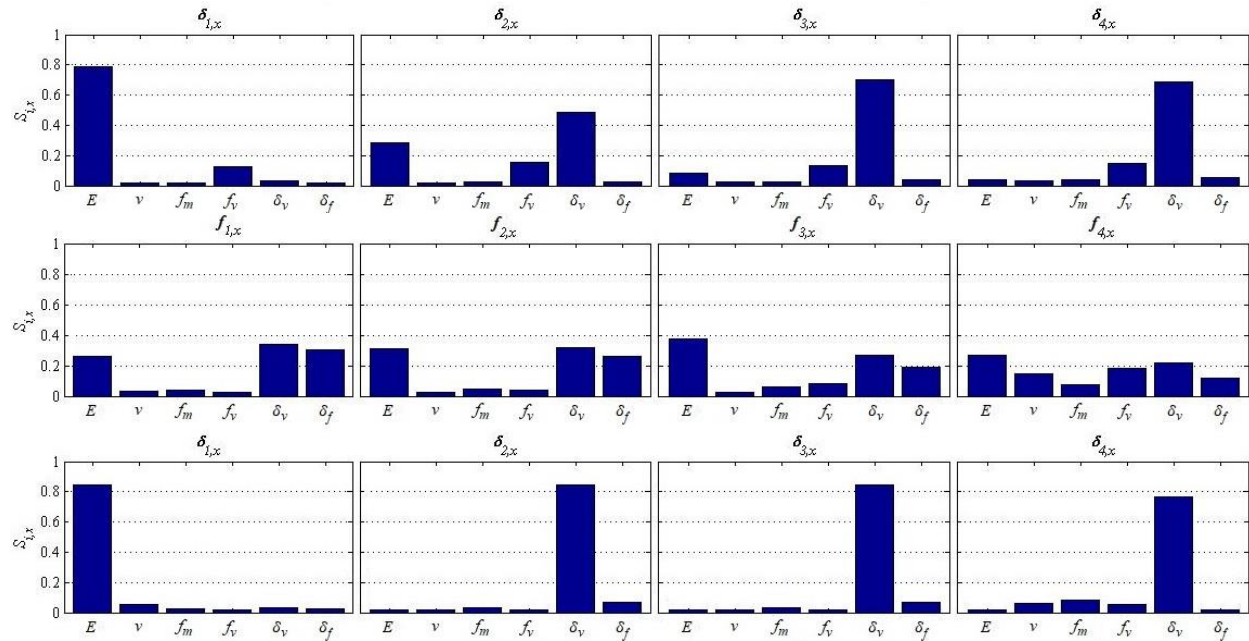


Fig. 22 - First-order sensitivity indices (Sobol, 1993) for the damage points of the archetypes A0 (2 up) and A7 (2 down).

7. Development of the Stochastic Models

Different methodologies may provide seismic damage intensities for fragility function fitting: hybrid methods, with seismic vulnerability analysis using damage matrices; simplified analytical methods, that use simplified formulas to assess the structural damage; and analytical methods, that use nonlinear static or dynamic analysis. The DSA uses the macromodel in Fig. 14, and its process may be followed in Fig. 23.

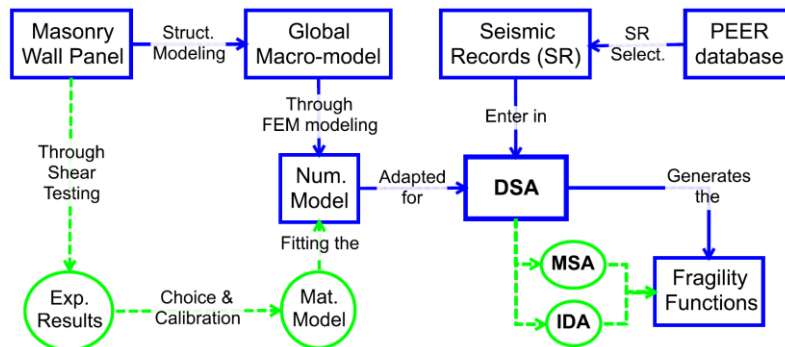


Fig. 23 – Conceptual map with work steps systematization of DSA [EC3].

The hybrid fragilities were achieved using vulnerability grades for buildings, facades and aggregates [51], following the concepts and empirical observations of the HBS, with reference on configuration of the archetypes A0 to A7. They show that despite the good conventional resistance (higher for shorter buildings), low slenderness and wall lengths, evenness of the openings, the type and quality of resisting system of the buildings, the plan regularity, and the position and foundations are disadvantageous. The damage measures *DM* (1 to 4) were defined in relatively to the vulnerability grades (1 to 5) for the expected damage in both buildings, facades and aggregates (Fig. 24).

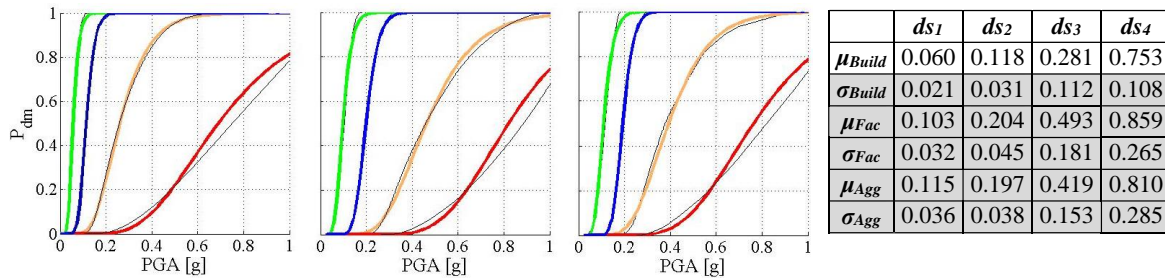


Fig. 24 – Fragility functions and respective moments, for buildings, facades and aggregates (from left to right).

The FEMA HAZUS fragilities were also studied [52], with moments for low and mid-rise URM buildings $\mu_{ds}=\{0.21\ 0.35\ 0.80\ 1.12\}$ and $\mu_{ds}=\{0.19\ 0.26\ 0.56\ 1.10\}$ respectively, with $\beta_{ds}=0.43$ [EC9].

The simplified Semi-empirical applications concerned both static and dynamic approaches, with the help of simplified mechanical models [20, 21]. The first, employed the CSM [27] and the latter IDA [28] (Fig. 23). The studies involve different estimates and assumptions, for instance [EC2, EC5], although the fragility moments present small variation (Fig. 24).

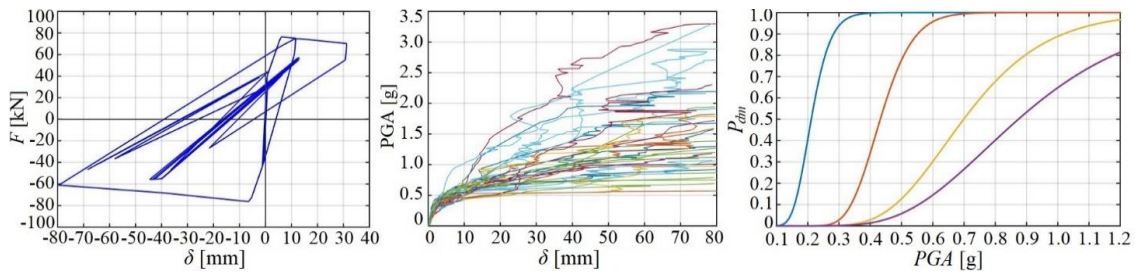


Fig. 25 – Dynamic analysis wall panel 8 subjected to one seismic record (left), IDA analysis in the δ -PGA axis (centre) & fragility functions (left), for wall panel 8.

The development of analytical fragility functions for the archetypes consisted on the application of both CSM, IDA and MSA to the archetypes from A0 to A7. The seismic nonlinear static analysis consisted on the application of the CSM was applied with $N_{sample}=100$. The DSA, utilized the simplified macro-model incorporating cyclic rigidity degradation. The resulting fragility curves can be seen in Fig. 26, with the respective statistical moments in Table 4.

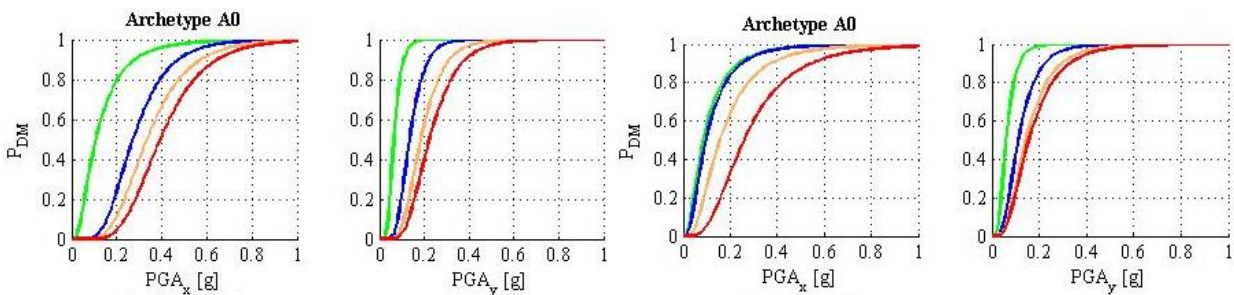


Fig. 26 – Fragility curves for the archetype A0, in both x and y direction, using the CSM (left) and IDA (right).

Table 4

Fragility moments for the archetypes A0 using CSM and IDA, and for archetype groups: A0 to A3, A4 to A7 and A0 to A7.

DS_i	CSM				IDA								MSA			
	A0				A0				A0 to A3		A4 to A7		A0 to A7			
	$\mu_{dsi,x}$	$\beta_{dsi,x}$	$\mu_{dsi,y}$	$\beta_{dsi,y}$	$\mu_{dsi,x}$	$\beta_{dsi,y}$	$\mu_{dsi,x}$	$\beta_{dsi,y}$	μ_{dsi}	β_{dsi}	μ_{dsi}	β_{dsi}	μ_{dsi}	β_{dsi}		
1	0.136	0.009	0.070	0.009	0.117	0.108	0.069	0.037	0.086	0.008	0.150	0.029	0.117	0.018	0.155	0.012
2	0.297	0.017	0.146	0.004	0.128	0.109	0.130	0.075	0.130	0.019	0.287	0.105	0.208	0.067	0.186	0.019
3	0.368	0.026	0.204	0.009	0.198	0.152	0.169	0.103	0.1663	0.033	0.357	0.187	0.259	0.109	0.255	0.010
4	0.427	0.031	0.253	0.014	0.306	0.196	0.186	0.118	0.247	0.059	0.422	0.083	0.342	0.106	0.265	0.009



The first-order sensitivity analysis of $Y=PGA_{dsi}$ considered the independent random variables are the material parameters, and the corner period T_C , and the maximum spectral acceleration normalized, calculated as $(S_{a,N})_{max} = S_{a,max}/PGA$, are arguably assumed as the earthquake parameters. The results divided two main groups (Fig. 27): (1) the earthquake parameters are relevant (the case of A4, A6 and A7), and (2) they are not especially significant, (the case of A0, A1, A2 and A3). Archetype A5 is found midway.

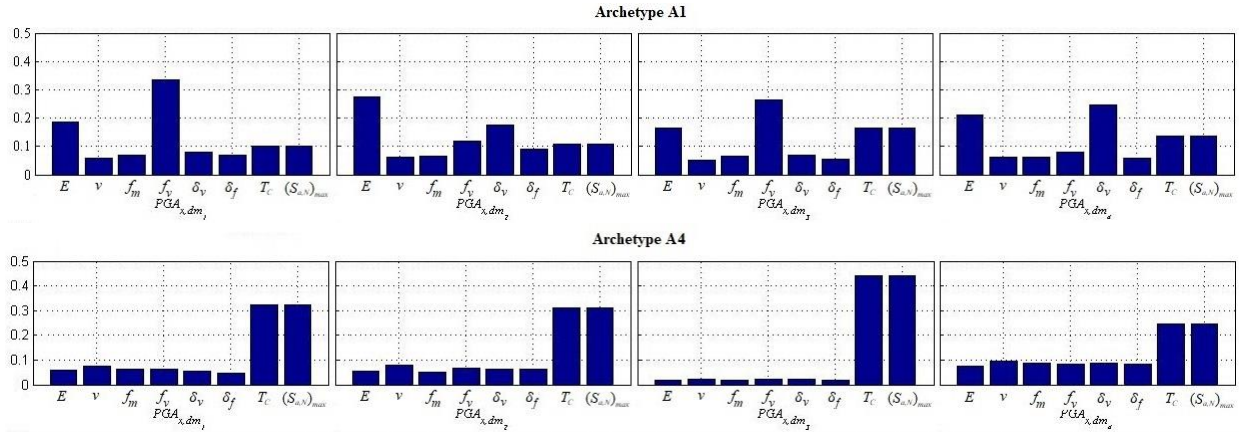


Fig. 27 – Sensitivity study of the damage points obtained by CSM, for the x direction of archetypes A1 and A7.

The results from IDA were studied using their correlation instead. The additional variables for this were the duration of the GM t , epsilon (ϵ), M is the moment magnitude and R the Joyner-Boore distance. The correlation coefficient is ρ_{X_i, Y_i} . The results are presented in Fig. 28.

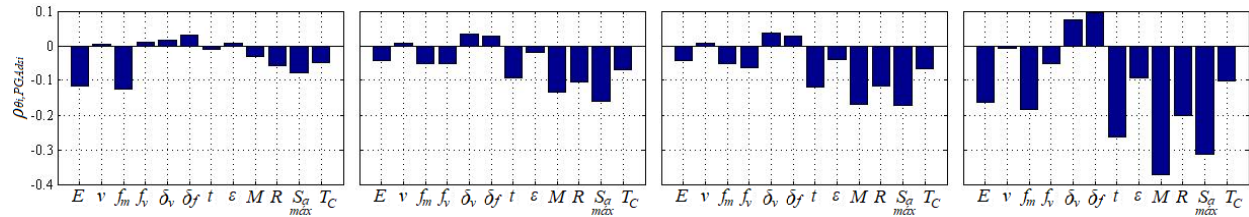


Fig. 28 - Study of the correlation between the damage PGA_{dsi} for archetypes A0 to A7 and the basic variables of the material model and of the selected earthquakes θ_i .

8. Magnitude Estimates for the 1763 Komárom Earthquake

The application of the magnitude estimation method is presented in two main groups: (1) first estimations, and (2) the final estimates, with the extended damage data set and final fragilities for Komárom.

The very first estimates tested the parametric uncertainty and sensitivity to assumptions using structural fragility functions attained by means of simplified mechanical models [EC4, EC9]. The framework assessed the impact of different fragility sets, attenuations, prior distance and magnitude models (Fig. 29, left & center) and damage sets. The results showed high influence of the magnitude priors (Fig. 29, right) and fragility means, but the negligible effect of the distance priors in the range $10 \leq R \leq 12$. The studies also suggested that the damages associated to the early fragility estimates [EC2, EC5], should have been a fraction of the total damage for Komárom. One conclusion is that general prior distributions, as Eq. (9) [11], should be used in order to assess building damage contributions. Nonetheless, the expected magnitude values ranged in between 6.23(0.12) and 7.11(0.52).



$$f_M(m) = \frac{1}{m_u - m_l}, \quad m_l \leq m \leq m_u \quad \& \quad f_R(r) = \frac{2}{r_u^2 - r_l^2} r, \quad r_l \leq r \leq r_u \quad (9)$$

where m_u, m_l and r_u and r_l , are the upper and lower bounds of magnitude and distance.

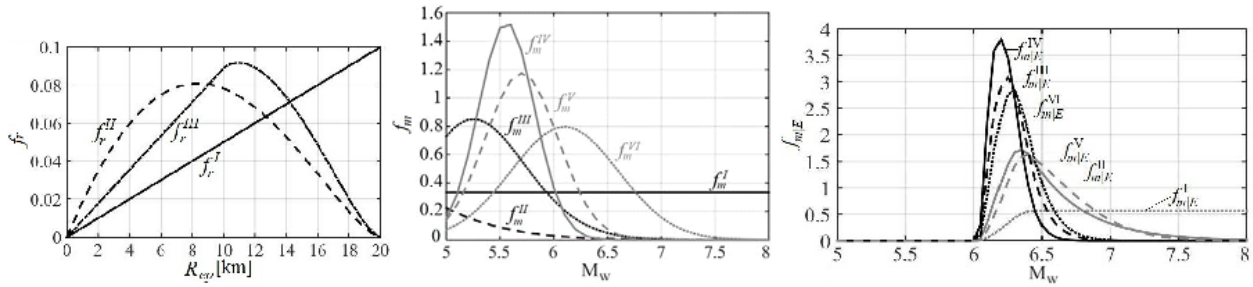


Fig. 29 – Prior distributions of distance (right), magnitude (center) and posterior distributions of magnitude (right), from Morais et al. (2018a).

The damage data was extended for the northern Danube bank by establishing a relationship between the repair costs (RC) and the number of damaged buildings ($DM\%$). Afterwards, the data was employed to study the correlation between damage and distance (R) with maximum correlation (possible epicenter) at $17.958^\circ/47.802^\circ$, in between the Eköll, Megyerets and Aranyos, similar result to [4]. The achievements are represented in Fig. 30.

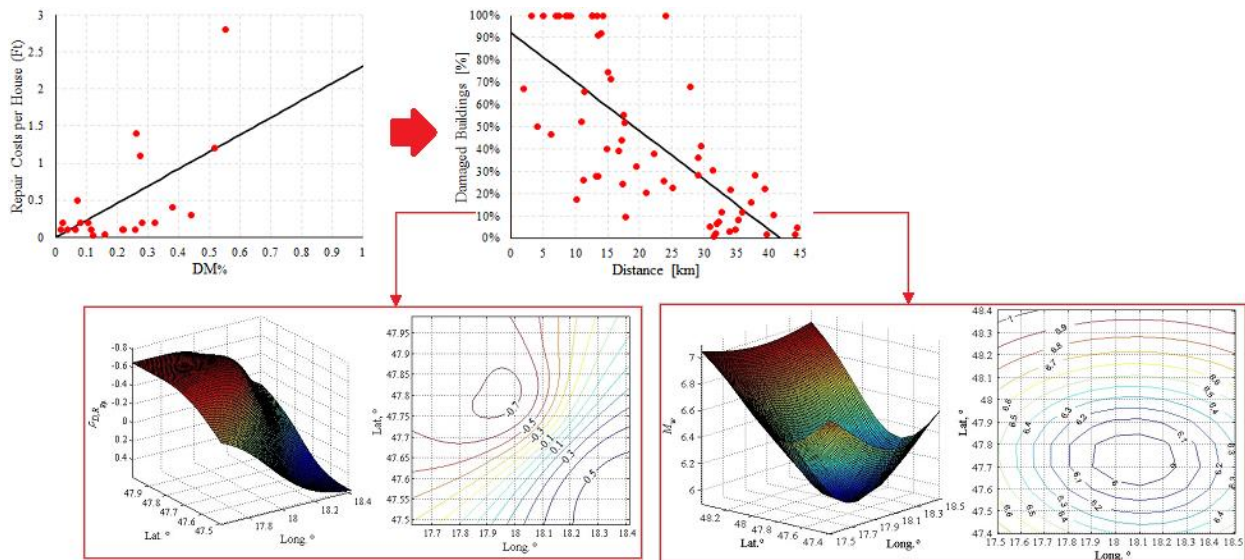


Fig. 30 – Simplified relationship between $DM\%$ and RC per house in Ft (up left), $DM\%$ per town and distances from $17.958^\circ/47.802^\circ$ (up right), correlations of the distance of the epicenter (down left) and magnitude estimates for buildings (down right).

The expected magnitude for multiple damage points. Additionally, the prior magnitude model was set as uniform in the range of feasible magnitudes $5 \leq M_w \leq 8$, the distance model was adapted following the precision of the distances and possible ranges, and the V_{s30} values were inputted for each site point [...]. The study utilized meshgrid and vulnerability curves for buildings, aggregates, and both CSM and IDA fragilities, for two locations of the epicenter $18.00^\circ/47.81^\circ$ and $17.958^\circ/47.802^\circ$, presenting similar expected values of magnitude $5.99 \leq \mu_{M|E} \leq 6.43$ and standard deviations $0.21 \leq \sigma_{M|E} \leq 0.33$, for the damage state ds_1 , described by hybrid, CSM and IDA fragilities. It is intriguing to observe that Győr and Komárom as the higher contributors, with $\mu_{M|E}$ above 7.00.

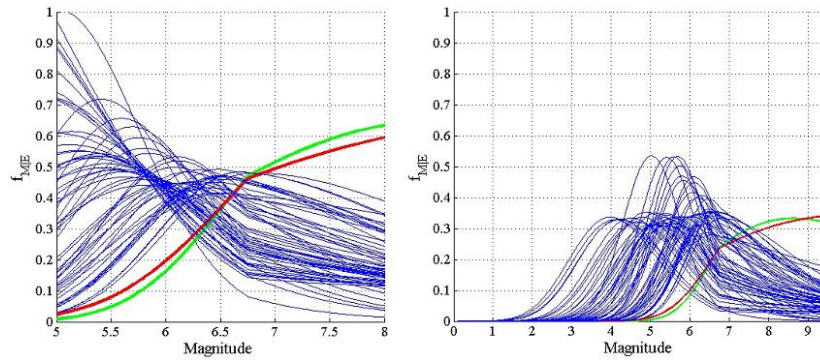


Fig. 31 - Resulting posterior distributions of magnitude for the fragilities obtained by CSM, for the epicenter in 18.00°/47.81°, with those of Győr (green) and Komárom (red) evidenced: in the magnitude ranges of $5 \leq M_w \leq 8$ (left) and of $0 \leq M_w \leq 9.5$ (right).

The damage data for the city of Komárom [4] may seem contradictory if we compare the typically expected frequency distributions of damage with the actually occurred damage (Fig. 32). The answer is probably on the vulnerabilities, as claimed by [10].

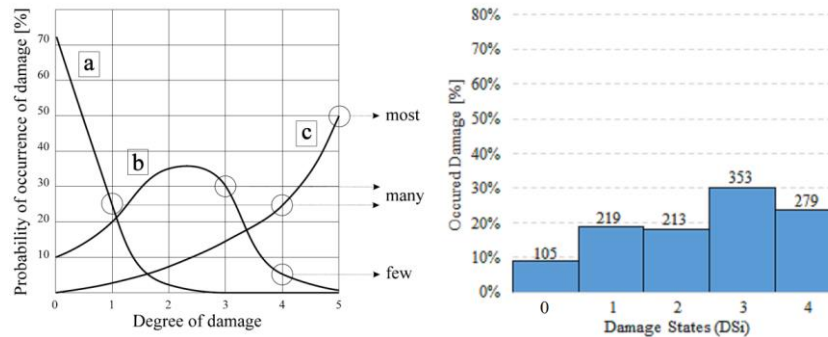


Fig. 32 – Relation between typical distributions of damage grades for different intensity degrees and definitions used in the presented intensity scale (EMS-98, 1998): [a] is $I=VI$, [b] for $I=VIII$ and [c] for $I=X$ (left) and damages in Komárom $n=1169$ (right).

Another observation points to Kastner’s drawing, highlighting the collapse of the gabled roofs [6]. The HBS has been used to determine the seismic coefficient c in terms of the equilibrium of the gables (Fig. 33). The damage PGAs were obtained using the GMR spectra and natural frequency T_n (s) assessed using [EN 1998]. The statistical moments presented a small variation between cases, and the mean for all cases and building classes were estimated as 0.193, and 0.022 the standard deviation.

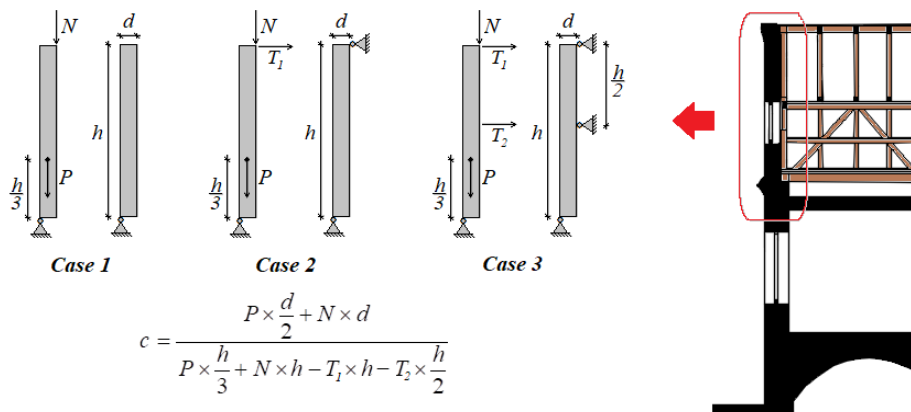


Fig. 33 - Possible support conditions for the Gable of the building ID 5 (Fig. 10).

The magnitude estimates for Komárom considered the detailed damage descriptions for the city. The fragilities obtained by IDA and MSA, described in four different damage states, were computed for magnitude estimation, with equal likelihood of occurring, resulting in the moments $\mu_{M|E}=6.41$ and $\mu_{M|E}=6.56$,



respectively, and $\sigma_{M|E}=0.74$ for both cases. The fragilities describing the collapse of the gables (0) were also computed. The expected magnitude value for having $\approx 50\%$ (139 buildings) of the collapses in the city is $\mu_{M|E}=6.53$, with $\sigma_{M|E}=0.74$, while the most probable value is 6.31. The results can be seen in Fig. 34, with the final estimates $\mu_{M|E}=6.48$ and $\sigma_{M|E}=0.75$.

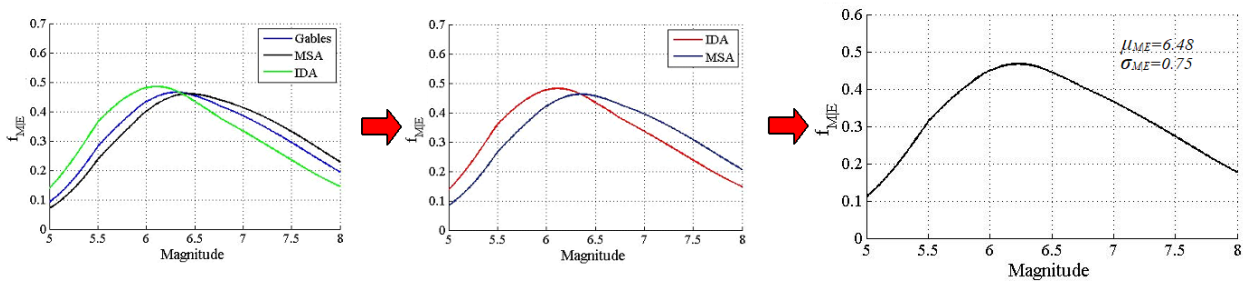


Fig. 34 –Posterior distributions of magnitude for the city of Komárom: for the overturn of the gables, IDA and MSA (left), the combination of the IDA and MSA with the overturn of the gables (center) and combination of the two previous scenarios (right).



9. New Scientific Results

9.1. Thesis I

I collected the historical damage and building descriptions related to the 1763 Komárom earthquake and the buildings survey of Tata, studying and interpreting them for the application of a structural engineering based magnitude estimation method. Historical claims were highlighted, stressed and extended on this sense. The following sub-steps were accomplished:

1. the depictions, drawings and descriptions of the buildings in Komárom were gathered and the buildings and damage typologies represented were gathered and studied for the application of a magnitude estimation method that uses structural engineering;
2. the damage states for the application of the magnitude estimation method were defined;
3. damages evidence sliding and diagonal shear, and rocking were observed in low-rise buildings along the collapse of the gables, while high-rise buildings evidence higher occurrences of flexural as rocking and toe-crushing and out-plane failure modes as different overturning of the gables, walls, chimneys, towers, and different forms of detachment of walls;
4. the claims of roof displacement and collapse of the gables have been confirmed, as sliding shear and overturning; the claim of higher damage in high-rise (taller) buildings was found plausible and likely given their relative higher mass;
5. the research endorses that the historical damage on the Zsámbék monastery church can not be straightforwardly associated to the 1763 earthquake, and therefore it should not be used as a case study for magnitude estimation.

Corresponding publications: Morais et al. (2014; 2016; 2017b; 2017d; 2018c)

9.2. Thesis II

I studied the building typologies of the 18th century Hungary in literature, inventoried and interpreted the historical building survey of the city of Tata in order to draw the typical historical baroque structural systems that already existed back in the 18th century from the surveyed buildings, evidencing that building categories and geometrical dimensions are associated. The following sub-steps were accomplished:

1. the main building categories, morphologies, geometries and structural systems were analysed regarding the literature and construction date, creating a database with their dimensions obtained from their 18th century structural elements;
2. a statistical analysis of the main dimensions of the walls evidences that local dwellings were lower, with smaller wall length and thickness than higher class nobleman, religious or even industrial buildings.

Corresponding publications: Morais et al. (2017c; 2018b)

9.3. Thesis III

I developed a methodology based on in-plane vulnerability indices, that uses both qualitative (arrangements, forms, construction date, type of structural elements) and quantitative frameworks (measurements and indices) to create historical building archetypes from historical building surveys. The method was adapted to the level of detail provided by the historical survey of Tata (1995) in order to study the 18th c. typologies. The following sub-steps were accomplished:



1. the outlines of the method were drawn targeting both the qualitative and quantitative features and framework necessary to generate historical building archetypes, using in-plane indexes as control parameters, thus extending their applicability;
2. 7 historical building archetypes (additionally to an earlier archetype A0) were generated using the methodology for four different building categories, associated to the historical descriptions and the survey;
3. the method also provides a pre-evaluation of the seismic safety of the buildings or relevant structural elements, evidencing the higher seismic resistance of local low-rise dwellings rather than higher-rise dwellings or nobleman, religious and industrial buildings; this aspect endorses point 2 of Thesis I.

Corresponding publications: Morais et al. (2017c; 2018b)

9.4. Thesis IV

I developed a simplified mechanical model for the efficient nonlinear analysis of unreinforced masonry, and calibrated and applied it to the building structural archetypes of Thesis III, providing both damage analysis and statistics associated to the variability of the mechanical parameters and ground motion, and with cyclic degradation. The following sub-steps were accomplished:

1. the archetypes and respective walls were modelled in both detailed and simplified macro-levels; detailed modelling techniques provided the force-displacement diagrams representing the seismic resistance of the archetypes, through static and dynamic analysis;
2. a simplified mechanical model was developed in OpenSees using a Pinching4 material to simulate the nonlinear dynamic behaviour and cyclic degradation of unreinforced masonry, calibrated using a genetic algorithm with the results from detailed methods;
3. the use of both nonlinear static and dynamic analysis shows the relevance of the latter to simulate the effect of cyclic [rigidity] degradation, providing lower ground motion intensities, thus affecting the magnitude estimates;
4. the sensitivity of the diagram points due to the variability of the parameters corroborates point 1 of Thesis I and point 2 of Thesis 3 by evidencing the impact of shear parameters in the archetypes A0 to A3, but also the impact of flexion parameters on A4 to A6.

Corresponding publications: Morais et al. (2018c)

9.5. Thesis V

The stochastic model was developed to fit lognormal seismic fragility functions adapted for the Komárom site, and given of the magnitude estimation of the 1763 Komárom earthquake evidencing the relevance of cyclic degradation in seismic analysis as well as both the ground motion and strength parameters variabilities. The following sub-steps were accomplished:

1. the force-displacement diagrams obtained by nonlinear analysis using the simplified model from Thesis IV were employed for efficient Dynamic Structural Analysis; fragility functions were produced for the archetypes comparing different methods, and incorporating uncertainties in material parameters and ground motion, as the Capacity Spectrum Method, and the Incremental Dynamic and Multiple Stripes Analyses;
2. the sensitivity and correlation studies show that the variability in ground motion is relatively more relevant to explain the variation in the seismic capacity of higher category archetypes (A4 to A7)



mainly) and for higher damage states than strength parameters, which are more relevant for lower category archetypes (A0 to A3) and lower damage states;

3. the fragility moments show the importance of the seismic degradation in the analysis of the archetypes, given that Capacity Spectrum Method provides relatively higher damage intensities than the Dynamic Analysis Methods after the calibration with sophisticated models.

Corresponding publications: Morais et al. (2016; 2017a; 2018c)

9.6. Thesis VI

I provided magnitude estimates and epicentral location for the 1763 Komárom earthquake using different approaches and assumptions frameworks. The combined analysis of the archetypes and gables updates and reinforces earlier estimates provided by Seismologists, with $M_w=6.48$ and probable epicenter in $18.00^\circ/47.81^\circ$. The following sub-steps were accomplished:

1. the number of damaged structures data can be extended for localities north to the Danube, using a simple relationship between damage and repair costs; a correlation study endorses the probable epicenter in $18.00^\circ/47.81^\circ$, corroborating literature in the field;
2. the magnitude estimation algorithm considering different damage points, one damage state and a new prior distribution of distance extends the original method but underestimates the magnitude, due to the low intensities associated with light damage;
3. given the damage descriptions, the fragilities from the dynamic analyses of the archetypes and gables, with a detailed hazard model for the city of Komárom, the expected magnitude of the 1763 earthquake is 6.48.

Corresponding publications: Morais et al. (2017a; 2018a)



Contributions of the Author

- [EC1] Morais E.C., Vigh L.G., Krähling J. (2014) Global response evaluation of a Hungarian Late Romanesque church due to a historical seismic event, *Proc. of the 2nd Int. Conf. of PhD Students in Civil Eng. and Arch.*, Cluj-Napoca, Romania, pp. 27–34.
- [EC2] Morais E.C., Vigh L.G., Krähling J. (2016) Fragility estimation and comparison using IDA and simplified macro-modelling of in-plan shear in old masonry walls, *Springer Proc. in Math. and Stat.*, Vol. 181, No. 1, pp. 277–291.
- [EC3] Vigh L.G., Rozsás A., Zsarnóczy A., Balogh T., Morais E.C., Simon J. (2016) Megbízhatósági analízis alkalmazása extrém hatásoknak kitett szerkezetek vizsgálatára, In: Hegedűs I., Farkas G., Dunai L., Kovács T., A BME Hidak és Szerkezetek Tanszék Tudományos Közleményei: Tassi Géza és Orosz Árpád 90 éves, 1st ed., *BME Hidak és Szerkezetek Tanszéke*.
- [EC4] Morais E.C., Vigh L.G., Krähling J. (2017) Preliminary estimation of the probable magnitude of Komárom 1763 earthquake using fragility functions, *Proc. of the 16th WCEE*, Santiago, Chile, 9-13 January, No. 4454, pp. 11.
- [EC5] Morais E.C., Vigh L.G., Krähling J. (2017) Seismic damage analysis of a Hungarian historical peasant house archetype, *Proc. of the 9th ENOC*, Budapest, Hungary, No. 509, pp. 6.
- [EC6] Morais E.C., Vigh L.G., Krähling J. (2017) Historical earthquakes and historical building archetypes for dynamic structural analysis using historical surveys, *Proc. of the 3rd PROHITECH*, Lisbon, Portugal, p. 12.
- [EC7] Sýkora M., Holický M., Markova J., Morais E.C., Diamantidis D. (2017) Compressive strength of historic masonry based on destructive and non-destructive test results, *Proc. of the 3rd PROHITECH*, Lisbon, Portugal, p. 10.
- [EC8] Morais E.C., Vigh L.G., Krähling J. (2017) Linear and non-linear seismic analysis of a Hungarian Late Romanesque church, *Acta Technica Napocensis*, Vol. 60, No. 1, pp. 42-58.
- [EC9] Morais E.C., Vigh L.G., Krähling J. (2018) Influence of prior distributions and fragility assessment methods in the estimation of the magnitude of a historical seismic event, *MATEC Web of Conf.*, Vol. 149, No. 1, p. 6.
- [EC10] Morais E.C., Vigh L.G., Krähling J. (2018) A methodology for the development of historical building archetypes for seismic performance assessment, *Pollack Periodica*, Vol. 13, No. 1, pp. 203-2015.
- [EC11] Morais E.C., Vigh L.G., Krähling J. (2018) Cyclic behavior, dynamic analysis and seismic vulnerability of historical building archetypes in Hungary, *Proc. of the 8th ICBR*, Lisbon, Portugal, pp. 11. (accepted manuscript)



References

- [1] Szeidovitz G. (1986) Earthquakes in the Region of Komárom, Mór and Várpalota, *Geophysical Transactions*, Vol. 32, pp. 255-274.
- [2] Szeidovitz G. (1990) Determination of epicentral intensity and focal depth of the earth-quakes occurred in the vicinity of Komárom and Mór (in Hungarian), *CSc Thesis*, MTA, Budapest, pp. 136.
- [3] Stucchi M. et al. (2013) The SHARE European Earthquake Catalogue (SHEEC) 1000-1899, *Journal of Seismology*, Vol. 17, No. 2, pp.524-544.
- [4] Varga P., Szeidovitz G., Gutdeutsch, R. (2001) Iseismal map and tectonical position of the Komárom earthquake of 1763, *Acta Geod. et Geoph. Hung.*, Vol. 36, No. 1, pp. 97-108.
- [5] Tóth L., Györgi E., Mónus P., Zsíros T. (2006) Seismic hazard in the Pannonian Region, In: Pinter N. et al. (eds), *The Adria microplate: GPS geodesy, tectonics and hazards. Nato Science Series: IV: Earth and Environmental Sciences*, Springer, Dordrecht, Vol. 61, pp. 369-384.
- [6] Broucek I., Eisinger U., Farkas V., Gutdeutsch R., Hammerl C., Szeidovitz G. (1990) Reconstruction of building damage caused by the 1763 earthquake in Komárno/Danube from contemporary depictions of the same site and from respective texts, *21st Gen. Ass. ESC*, Barcelona, Spain, pp. 353–363.
- [7] Eisinger U., Gutdeutsch R., Hammerl, C. (1992) Historical Earthquake Research, an example of interdisciplinary cooperation between geophysicists and historians, *Abh. Geol. B.-A.*, Vol. 1, pp. 33-50.
- [8] Medvedev J. (1962) Engineering Seismology, *Academia Nauk Press*, Moscow.
- [9] MNL OL N-98 (1763) Acta Terrae motus anni 1763, Ladula CCC, Fascisculus A–E.
- [10] Grossinger J. (1783) Dissertatio de terrae motibus regni Hungariae, excerpta ex universa historia physica Hung. manuscripta, Győr, *Jaurini*.
- [11] Ryu H., Kim J., Baker J. (2009) A Probabilistic method for the magnitude estimation of a historical damaging earthquake using structural fragility functions, *Bull. Seism. Soc. of Am.*, Vol. 99. No. 2A pp. 520-537.
- [12] Istvánfi G. (1995) Surveys of settlements completed during the summer stages for students of architecture between 1980 and 1994, (in Hungarian) Budapest University of Technology and Economics, *Institute of Theory and History of Architecture*, Budapest, Hungary.
- [13] Halmos B., Marótyz K. (2010) The Adaptations of the true-to-form survey method, *Periodica Polytechnica*, Vol. 41, No. 1, pp. 9-17.
- [14] Genthon I. (1959) Magyarország Műemlékei, *Akadémiai Kiádo*.
- [15] Rados J. (1964) Tata, *Műszaki Könyvkiadó*, pp. 223.
- [16] Haris A., Somorjay S. (2006) Magyarország műemlékjegyzéke: komárom–esztergom megye, Kulturális Örökségvédelmi Hivatal, Budapest.
- [17] Lourenço P.B., Roque J.A. (2006) Simplified indexes for the seismic vulnerability of ancient masonry buildings, *Construction and Building Materials*, pp. 200-208.
- [18] Lourenço P.B., Oliveira D.V., Leite J.C., Ingham J.M., Modena C., da Porto F. (2013) Simplified indexes for the seismic assessment of masonry buildings: International database and validation, *Engineering Failure Analysis*, Vol. 34, No. 1, pp. 585–605.
- [19] Stucchi M. (1993) Historical seismology and earthquake hazard, *Annali di Geofisica*, Vol. 36, No. 1, pp. 177-189.
- [20] FEMA P-368 (2003) NEHRP recommended provisions for seismic regulations for new buildings and other structures, Part1: provisions, Report n° 368, *FEMA*, Washington DC.
- [21] Rafsanjani S.H., Bakhshi A., Ghannad M.A., Yekrangnia M., Soumi F. (2015) Predictive tri-linear benchmark curve for in-plane behavior of adobe walls, *International Journal of Architectural Heritage*, Vol. 9, No. 8, pp. 986-1004.
- [22] Lagomarsino S., Penna A., Galasco A., Cattari S. (2013) TREMURI Program: an equivalent frame model for the nonlinear seismic analysis of masonry buildings, *Engineering Structures*, Vol. 56, No. 11, pp. 1787-1799.



- [23] Mckenna F., Fenves G., Scott M., Jeremic B. (2006) Open system for earthquake engineering simulation (OpenSees), Berkeley, CA.
- [24] Inter-CAD Kft (2018) AxisVM-X4: User's manual, Budapest, Hungary, pp. 506.
- [25] Cervenka V., Jendele L., Cervenka J. (2016) *ATENA program documentation part 1: Theory*, Prague, Czech Republic.
- [26] Lourenço P.B. (2001) Analysis of historical constructions: from thrust-lines to advanced simulations, In: *Historical constructions*, P.B. Lourenço, P. Roca (eds.), Guimarães, pp. 91-116.
- [27] Freeman S.A. (1998) Development and use of capacity spectrum method, *Proceedings of the 6th US National Conference on Earthquake Engineering*, Seattle, Washington, U.S.A.
- [28] Vamvatsikos D., Cornell C.A. (2004) Applied incremental dynamic analysis, *Earthquake Spectra*, Vol. 20, No. 2, pp. 523–553.
- [29] Jalayer F., Cornell C.A. (2009) Alternative nonlinear demand estimation methods for probability-based seismic assessments, *Earthquake Eng. & Struct. Dyn.*, Vol. 38, No. 8, pp. 951-972
- [30] Woessner J., Laurentiu D., Giardini D., Crowley H., Cotton F., Grünthal G., Valensise G., Arvidsson R., Basili R., Demircioglu M.B., Hiemer M., Meletti C., Musson R.W., Rovida A.N., Sesetyan K., Stucchi M. (2015) The 2013 European seismic hazard model: key components and results, *Bulletin of Earthquake Engineering*, Vol. 13, pp. 3553–3596.
- [31] MVM Paks II Ltd. (2016) Geology, geophysics, seismology, geotechnics and hydrology [in Hungarian], *Site Safety Analysis Report*, Vol. 2, No. 5, pp. 197.
- [32] Akkar S., Sandikkaya M.A., Bommer J.J. (2013) Empirical ground-motion models for point- and extended-source crustal earthquake scenarios in Europe and the Middle East, *Bulletin of Earthquake Engineering*, Vol. 12, No. 1, pp. 359-387.
- [33] Augenti N., Parisi F., Acconcia E. (2012) MADA: Online experimental database for mechanical modelling of existing masonry assemblages, *15th WCEE*, Lisbon, Portugal.
- [34] Caporale A., Parisi F., Asprone D., Luciano R., Prota A. (2015) Comparative micromechanical assessment of adobe and clay brick masonry assemblages based on experimental data sets, *Composite Structures*, Vol. 120, No. 1, p. 208-220.
- [35] Csicsely A. (2006) Experimental and theoretical capacity of mud walls (in Hungarian), *PhD dissertation*, BME, Budapest, Hungary, 2006.
- [36] Ruiz S., *Seismic risk assessment of adobe dwellings*, MSc thesis, Instituto Universitario di Studi di Pavia, Pavia, Italy, 2008.
- [37] Minke G. (2001) *Construction manual for earthquake-resistant houses built of earth*, GTZ, 2001.
- [38] Choi S., Grandhi R.V., Canfield R.A. (2007) *Reliability-based Structural Design*, Springer, London.
- [39] Grünthal G. (1998) European macroseismic scale, *European Center for Geodynamics and Seismology*, Luxembourg, pp. 101.
- [40] Réthly A. (1952) Earthquakes in the Carpathian Basin (in Hungarian), *Akadémiai Kiadó*.
- [41] Timár G., Biszak S., Székely B., Molnár G. (2011) Digitized maps of the Habsburg military surveys, Overview of the project of ARCANUM Ltd. (Hungary), In: Jobst M. (eds.), *Preservation in digital cartography, Lecture Notes in Geoinformation and Cartography*, Springer, Berlin, pp. 273–283.
- [42] EN 1996-1-1 (2005) Eurocode 6: design of masonry structures - part 1-1: common rules for reinforced and unreinforced masonry structures, *European Committee for Standardization*, Brussels.
- [43] EN 1998-1 (2004), Eurocode 8: design of structures for earthquake resistance, part 1: general rules, seismic actions and rules for buildings, *European Committee for Standardization*, Brussels.
- [44] Lourenço P.B., Fernandes F., Castro F. (2010) Handmade clay bricks: chemical, physical and mechanical properties, *International Journal of Architectural Heritage*, Vol. 4, No. 1, pp. 38-58.
- [45] KJM-ML (1898) Deliverable of the Mechanics Laboratory of the King Joseph Technical University, Booklet III: Roman cement, Portland cement and other mortar materials (in Hungarian), pp. 75.



- [46] Laefer D.F., Boggs J., Cooper N. (2004) Engineering properties of historic brick: variability considerations as a function of stationary versus nonstationary kiln types, *Journal of the American Institute for Conservation*, Vol. 43, No. 3, pp. 255-272.
- [47] Allen T.I., Wald D.J. (2009) On the use of high-resolution topographic data as a proxy for seismic site conditions (V_{S30}), *Bull. of the Seism. Soc. of Am.*, Vol. 99, No. 2A, pp. 935-943.
- [48] Ptilakis K. (2004) Site effects, In: Ansal A. (ed.) *Recent advances in earthquake geotechnical engineering and microzonation*, Kluwer, Dordrecht, pp. 139–197.
- [49] PEER (2013) NGA-West2 Ground Motion Prediction Equations for Vertical Ground Motions. PEER Report 2013/24, *Pacific Earthq. Eng. Research Center*, University of California, Berkeley, CA.
- [50] Vigh L.G., Liel A.B., Deierlein G.G., Miranda E. (2014) Tipping S., Component model calibration for cyclic behaviour of a corrugated shear wall, *Thin-Walled Structures*, Vol. 75, pp. 53-62.
- [51] Vicente, R.S. (2008) Strategies and Methodologies for the interventions and urban rehabilitation (in Portuguese), *PhD Dissertation*, Universidade of Aveiro, Aveiro, Portugal.
- [52] HAZUS-MH MR-1 (2003) Technical Manual, *FEMA*, Washington D.C.